Development of the Cylindrical Wire Electrical Discharge Machining Process, Part 1: Concept, Design, and Material Removal Rate

Jun Qu
Research Assistant

Albert J. Shih
Associate Professor

Department of Mechanical and Aerospace Engineering, North Carolina State University, Raleigh, NC 27695

Ronald O. Scattergood
Professor
Department of Materials Science and Engineering, North Carolina State University, Raleigh, NC 27695

Results of applying the wire Electrical Discharge Machining (EDM) process to generate precise cylindrical forms on hard, difficult-to-machine materials are presented. The design of a precise, flexible, and corrosion-resistant underwater rotary spindle is first introduced. A detailed spindle error analysis identifies the major sources of error at different frequency spectrum. The spindle has been added to a conventional two-axis wire EDM machine to enable the generation of free-form cylindrical geometries. The mathematical model for material removal rate of the free-form cylindrical wire EDM process is derived. Experiments were conducted to explore the maximum material removal rate for cylindrical and 2D wire EDM of carbide and brass work-materials. Compared to the conventional 2D wire EDM of the same work-material, higher maximum material removal rates may be achieved in the cylindrical wire EDM, possibly due to better debris flushing condition. [DOI: 10.1115/1.1475321]

1 Introduction

Electrical Discharge Machining (EDM) is a thermoelectric process that erodes workpiece material by a series of discrete electrical sparks between the workpiece and an electrode flushed by or immersed in a dielectric fluid. Unlike traditional cutting and grinding processes, which rely on the force generated by a harder tool or abrasive material to remove the softer work-material, the EDM process utilizes electrical sparks or thermal energy to erode the unwanted material and generate the desired shape. The hardness and strength of the difficult-to-machine work-materials are no longer the dominating factors that affect the tool wear and hinder the machining process. This makes the EDM process particularly suitable for machining hard, difficult-to-machine materials. The EDM process has the ability to machine precise, complex, and irregular shapes with a CNC control system. In addition, the cutting force in the EDM process is small, which makes it ideal for fabricating parts with miniature features.

The concept of cylindrical wire EDM is illustrated in Fig. 1. A rotary axis is added to a conventional two-axis wire EDM machine to enable the generation of a cylindrical form. The initial shape of the part needs not to be cylindrical in shape. The electrically charged wire is controlled by the X and Y slides to remove the work-material and generate the desired cylindrical form. An example of the diesel fuel system injector plunger machined using the cylindrical wire EDM method is shown in Fig. 2.

The idea of using wire EDM to machine cylindrical parts has been reported by Dr. Masuzawa's research group at University of Tokyo [1–8]. These research activities were aimed to manufacture small-diameter pins and shafts. A wire guide was used to reduce the wire deflection during EDM of small-diameter shafts. Cylindrical pins as small as 5 μm in diameter can be machined [8]. The small-diameter pins can be used as tools for 3D micro-EDM applications [9,10].

In this study, instead of machining small-diameter pins, the focus is on exploring high material removal rates in the cylindrical wire EDM process. The material removal rate data was not reported in Masuzawa's research [1–8]. In this study, two configurations to find the maximum material removal rate for cylindrical wire EDM were explored. One of the difficult-to-machine metal matrix ceramic composites, tungsten carbide in cobalt matrix, was used in this study. The mathematical model for material removal rate was derived to help understand and improve the cylindrical wire EDM process.

The spindle design and spindle error analysis methods are first presented in this paper. The model of material removal rate in free-form cylindrical wire EDM is then derived. Finally, the experimental results of the maximum material removal rates in the cylindrical wire EDM process are analyzed and compared to that of 2D wire EDM.

2 Spindle Design

The rotating workpiece is driven by a spindle, which is submerged in a tank of deionized water. Two jets of high-pressure water are used to flush the workpiece to improve the material removal rate and maintain a uniform thermo-environment. A precision underwater spindle is the key subsystem of the experiment. This spindle must meet the following design criteria:

1. *Accuracy*: The spindle error needs to be small to machine accurate parts and maintain the consistent gap condition.
2. *Flexibility*: The spindle has to accommodate different sizes of workpiece.
3. *High Current Electrical Connection*: Wire EDM requires high-current, high-voltage electrical connections between the rotating workpiece and the ground. A back-wired carbon electrical brush is required for the electrical connection to the rotating workpiece.
4. *Corrosion Resistance*: Because the spindle is underwater, components of the spindle need to be corrosion resistant in water.

The picture of the underwater spindle used in this study is shown in Fig. 3, respectively. A pair of deep groove silicon nitride ball bearings with stainless steel rings was used. The gear

Contributed by the Manufacturing Engineering Division for publication in the JOURNAL OF MANUFACTURING SCIENCE AND ENGINEERING. Manuscript received May 2001; Revised December 2001. Associate Editor: Y. L. Yao.

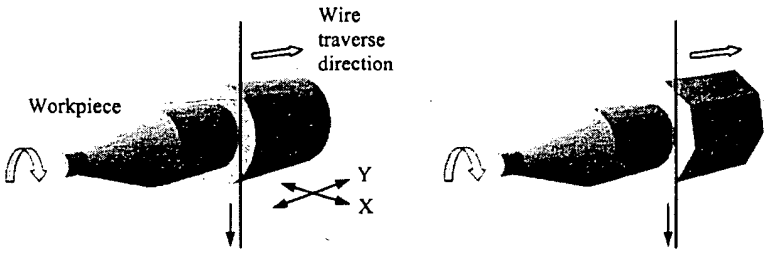

Fig. 1 The concept of cylindrical wire EDM process

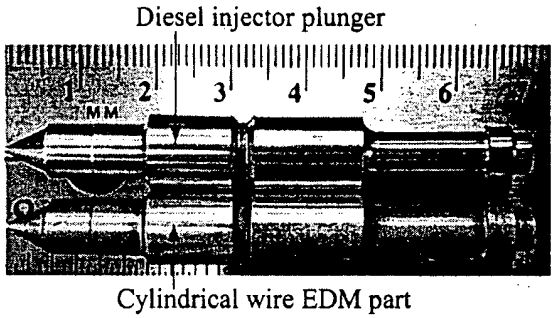

Fig. 2 A cylindrical wire EDM part with the same shape as the diesel engine injector plunger

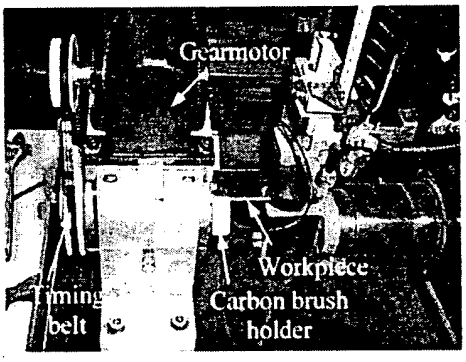

Fig. 3 Side view of the hybrid bearing underwater spindle

motor was located above water on the top of the frame. A timing belt was used to transmit the rotational motion to the R8 collet holder. Precision internal grinding of the angle in the collect holder was required to achieve the desired runout specification, which is less than 10 μm on the part 20 mm from the face of the collet.

3 Spindle Error Analysis

Spindle runout error is an important parameter that can affect the maximum material removal rate, roundness, and surface finish of cylindrical wire EDM parts. The Donaldson reversal principle [11] was applied to measure the spindle error. An electronic indicator with 0.1 μm resolution was used to measure two runout traces on opposite sides of a 6.35 mm diameter silicon-nitride bar. The spindle error can be calculated from these two runout traces. A sample spindle error trace at 30 rpm is shown in Fig. 4. The maximum spindle error is defined as the average peak to valley value on the error trace. Results of the maximum spindle error at 10 different speeds are shown in Fig. 5. Fourier transformation was applied to analyze the spindle runout data to identify the source of error. Figure 6 shows the amplitude of error vs. frequency for two spindle rotational speeds at 30 and 60 rpm. Four major peaks can be identified.

(i) f_0: This is the major peak, which is caused by the off center error. The position of this peak always corresponds to the spindle rotational speed.

(ii) f_1: This is always equal to five times the rotational speed of the spindle, possibly caused by the form error on bearing races.

(iii) f_3 and f_4: These two frequencies, 60 and 120 Hz, remain unchanged for different motor rotational speeds. The frequency peak at 120 Hz is possibly caused by the DC motor. The amplitude of the frequency at 60 Hz is only significant at certain motor rotational speeds, such as 90 and 180 rpm. This is possibly caused by resonance at the spindle's natural frequency, which is measured as 60 Hz.

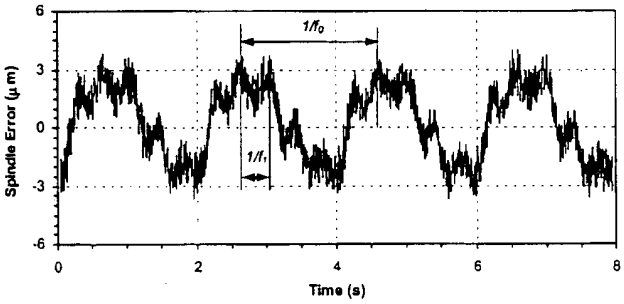

Fig. 4 Spindle error at 30 rpm rotational speed

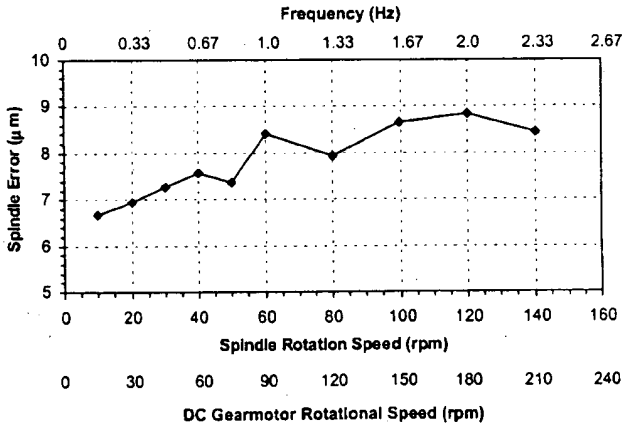

Fig. 5 Spindle error vs. rotational speed

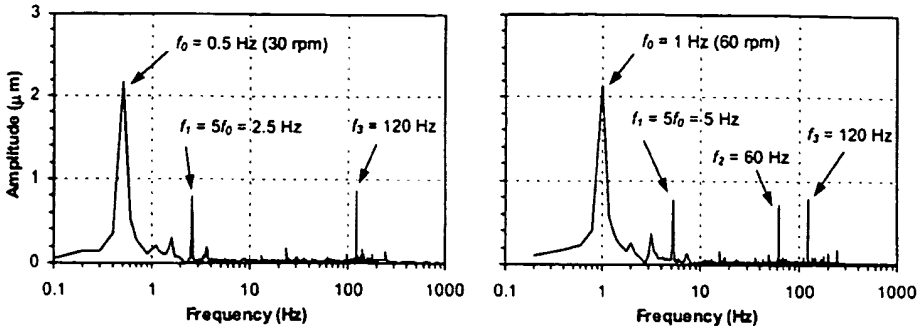

(a) Spindle rotation speed of 30 rpm (b) Spindle rotation speed of 60 rpm

Fig. 6 FFT Frequency spectrum of the spindle error

4 Material Removal Rate Modeling

The process parameters for modeling the material removal rate in cylindrical wire EDM of a free-form shape are illustrated in Fig. 7. An XY coordinate system is first defined. The X-axis coincides with the rotational axis of the workpiece. The positive direction of the X-axis is determined by the direction of the wire traverse velocity vector, v_f. The component of the wire-traverse velocity vector on the X-axis is always positive. The Y-axis, in the radial direction of the cylindrical workpiece, is perpendicular to both the X-axis and the wire. Assume the original workpiece is in cylindrical geometry. R is the original radius of the workpiece. r_e is the radius of the effective circle, C_e, which equals the wire radius, r_w, plus the width of the gap between the wire and the workpiece. r is the minimum distance from the effective circle, C_e, to the rotational axis of the workpiece. v_f, the magnitude of v_f, is equal to the wire feed rate during machining. α is the angle from the positive X-axis to v_f. The range of α is from $-\pi/2$ to $\pi/2$.

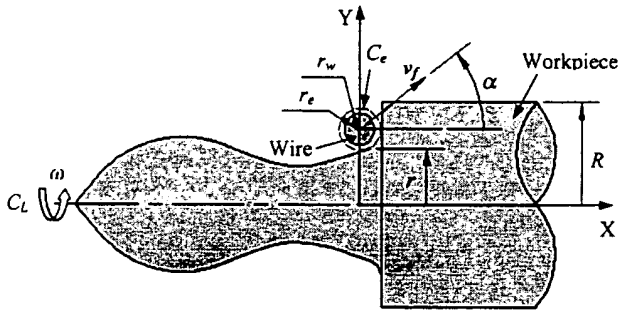

Fig. 7 Parameters in the free form cylindrical wire EDM process

Table 1 Machine setup for the cylindrical wire EDM experiment

Wire EDM machine	Brother HS-5100	
Wire manufacturer	Charmilles Technologies, BercoCut	
Wire material	Brass	
Wire diameter (mm)	0.25	
Workpiece material	Brass	Carbide
Spark cycle (μs)	20	28
On-time (μs)	14	14
(Duty factor, On-time/Spark Cycle)	(70%)	(50%)
Axial direction wire speed (mm/s)	15	18
Wire tension (N)	14.7	14.7
Gap voltage (V)	45	35

The Material Removal Rate (MRR) in cylindrical wire EDM of a free-form cylindrical geometry is shown in Eq. (1) with the detailed derivation summarized in the Appendix.

$$MRR = v_f \cdot \pi \left[(R^2 - r^2)\cos\alpha + 2rr_e(1 - \sin\alpha - \cos\alpha) + r_e^2\left(2 - 2\cos\alpha + \left(\frac{\pi}{2} - 2 - \alpha\right)\sin\alpha\right)\right] \quad (1)$$

5 Experiment on the Maximum Material Removal Rate

Two types of materials, carbide and brass, were used in this study. The carbide material is 1 to 2 μm size tungsten carbide in a 10% cobalt matrix. This material has hardness of 92 Rc, transverse rupture stress of 3.4 MPa, and specific density of 14.5. The brass material is alloy 360 free-machining brass with 61.50% copper, 35.25% Zinc, and 3.25% lead. Relative to the carbide, brass is easy to EDM because of its good electrical conductivity and low melting temperature. The machine setup and process parameters for the cylindrical wire EDM experiment are listed in Table 1. Two parameters, the part rotational speed, ω, and wire feed rate, v_f, are varied in this study to investigate their effect on the cylindrical wire EDM of two different work-materials. Results of the maximum material removal rate are discussed below.

The maximum material removal rate (MRR_{max}) is an important indicator of the efficiency and cost-effective of the process. Tests are designed to find the MRR_{max} in both the cylindrical and 2D wire EDM. Two test configurations to measure the MRR_{max} in cylindrical wire EDM are illustrated in Figs. 8(*a*) and 8(*b*). Two 2D wire EDM tests, as shown in Figs. 8(*c*) and 8(*d*), were also conducted on the same work-material to evaluate the difference in MRR_{max}.

Key parameters of the two configurations to find the MRR_{max} in cylindrical wire EDM are shown in Fig. 9. In Fig. 9(*a*), α is set to 0 degree and v_f is gradually increased to the limiting speed, when the short circuit error occurs. This v_f is recorded as $v_{f,max}$ and the MRR_{max} can be calculated using Eq. (1). Another test configuration to measure MRR_{max} in cylindrical wire EDM, as shown in Fig. 9(*b*), has constant α and v_f. As the wire cuts into the workpiece, the material removal rate is gradually increased. At the position when the short circuit error occurs, the material removal rate is recorded as MRR_{max}. Two test configurations to find MRR_{max} for 2D wire EDM at different thickness are shown in Figs. 8(*c*) and 8(*d*). The v_f was gradually increased to find the MRR_{max}. Results of MRR_{max} are summarized in Tables 2 to 4.

Several observations can be extracted from the data in Tables 2 to 4.

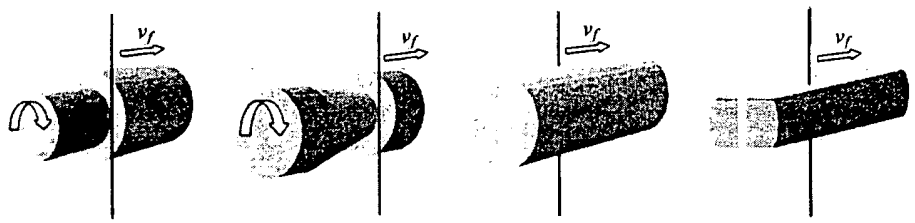

(a) Cylindrical test I (b) Cylindrical test II (c) 2D test I (d) 2D test II

Fig. 8 Four test configurations to find the maximum material removal rate

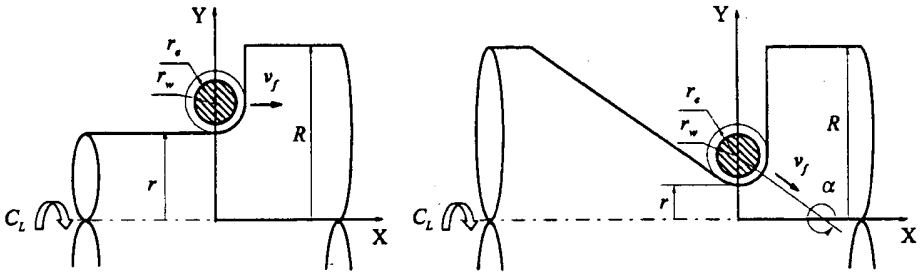

(a) $\alpha = 0$ and gradually increasing v_f (b) constant α and v_f

Fig. 9 Key parameters of the two configurations to find the maximum material removal rate in cylindrical wire EDM

Table 2 MRR_{max} for the cylindrical wire EDM test with $\alpha=0$ and gradually increasing v_f

Material	R (mm)	3.18			2.54	
	r (mm)	2.54	1.59	0.75	1.59	0.75
Brass	$v_{f,max}$ (mm/min)	5.72	2.69	2.13	5.33	3.46
	MRR_{max} (mm³/min)	65.2	64.1	63.7	65.7	64.0
Carbide	$v_{f,max}$ (mm/min)	1.42	0.81	0.66	1.55	1.02
	MRR_{max} (mm³/min)	16.2	19.3	19.7	19.1	18.9

Table 3 MRR_{max} for the cylindrical wire EDM test with constant α and v_f

Material	v_f (mm/min)	α (degree)	-15	-30	-45
Brass	3.81	r_{min} (mm)	2.16	2.01	1.65
		MRR_{max} (mm³/min)	65.5	68.3	69.6
Carbide	1.02	r_{min} (mm)	2.02	1.95	1.17
		MRR_{max} (mm³/min)	19.1	18.7	20.9

Table 4 MRR_{max} for the 2D wire EDM test

Material	Thickness (mm)	r_e (mm)	$v_{f,max}$ (mm/min)	MRR_{max} (mm³/min)
Brass	6.35	0.183	23.9	55.5
	3.23	0.183	37.8	44.7
Carbide	6.35	0.163	4.32	8.94
	3.23	0.163	8.00	8.42

1. The brass has much higher material removal rate than the carbide.
2. The MRR_{max} for cylindrical wire EDM in Tables 2 and 3 is greater than the 2D wire EDM results in Table 4. The possible cause may be better flushing conditions in the cylindrical wire EDM. In 2D wire EDM, as shown in Fig. 8(*c*), a narrow gap exists and affects the flow of high-pressure water jets for flushing. Such situation does not exist in the cylindrical wire EDM.
3. The MRR_{max} for 2D wire EDM changes slightly with thickness.
4. For carbide, the MRR_{max} may not be as high as that in rough grinding. However, this process does provide the advantage in flexibility to shape the workpiece.
5. The results from the two test configurations for cylindrical wire EDM at different sizes and angles are close to each other. The maximum material removal rate is calculated using the material removal rate model under various process setup parameters. This has verified the concept and mathematical model for the material removal rate.

Another important observation in this experiment is: the wire breakage is more likely to occur during cutting at a steeper angle α in the test configuration shown in Fig. 9(*b*).

6 Concluding Remarks

The feasibility of applying the cylindrical wire EDM process for high material removal rate machining of free-from cylindrical

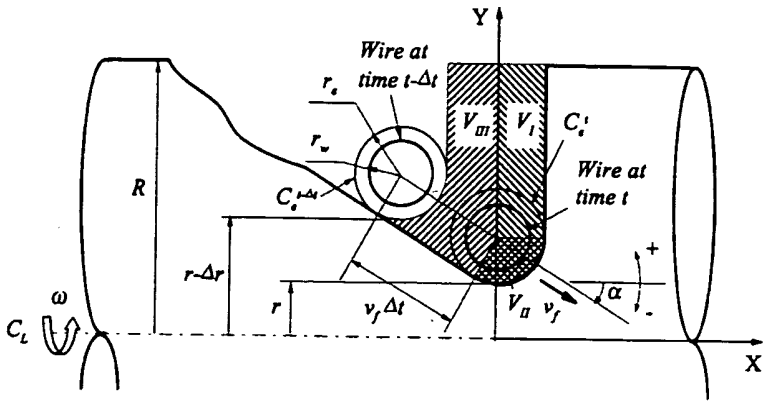

Fig. 10 Free form geometry in cylindrical wire EDM

geometries was demonstrated in this study. The mathematical model for the material removal rate of cylindrical wire EDM of free-form surfaces was derived. Two experimental configurations designed to find the maximum material removal rates in cylindrical wire EDM were proposed. Results of each test configurations match each other. The maximum material removal rate for the cylindrical wire EDM was higher than that in 2D wire EDM of the same work-material. This indicates that the cylindrical wire EDM is an efficient material removal process.

The spindle was found to be a critical factor in achieving the desired roundness, surface finish, and material removal rate. The effect of spindle error on part roundness will be discussed in the following paper. Other refinements to enhance the spindle accuracy are required to achieve better cylindrical wire EDM results. One of the advantages of the cylindrical wire EDM process is its ability to machine micro-size shafts. Preliminary results indicated that a precision spindle is the key factor in the system for micro-machining applications.

Acknowledgment

The authors gratefully acknowledge the support by National Science Foundation Grant #9983582 (Dr. K. P. Rajurkar, Program Director). Portion of this research was sponsored by the User program in the High Temperature Material Lab, Oak Ridge National Lab and the Heavy Vehicle Propulsion Systems Materials Program, Office of Transportation Technologies, US Department of Energy. The assistance from Darryl Gust of Cummins Technical Center on the design and manufacture of the spindle is also greatly appreciated.

Appendix

Material Removal Rate Modeling in Cylindrical Wire EDM. The mathematical model of Material Removal Rate (*MRR*) in cylindrical wire EDM of a free-form shape is presented. This is a geometrical model, which does not include the process parameters, such as voltage and current. Figure A1 shows the free-form cylindrical geometry machined by the cylindrical wire EDM process. The effective circles of the wire at time $t-\Delta t$ and t are represented by $C_e^{t-\Delta t}$ and C_e^t, respectively. Δr is the change of r during Δt, and can be expressed as:

$$\Delta r = v_f \Delta t \cdot \sin\alpha \qquad (A.1)$$

The volume of the material removed from $t-\Delta t$ to t is denoted as V. As shown in Fig. 10, V is the volume swept by the hatched area around the X-axis. V can be divided into three portions, $V_{\rm I}$, $V_{\rm II}$, and $V_{\rm III}$.

$$V = V_{\rm I} + V_{\rm II} + V_{\rm III} \qquad (A.2)$$

$V_{\rm I}$ is a ring with outer radius R, inner radius $r+r_e$, and thickness r_e.

$$V_{\rm I} = \pi[R^2 - (r+r_e)^2]r_e \qquad (A.3)$$

An enlarged figure of the volume $V_{\rm II}$ is shown in Fig. 11.

$$V_{\rm II} = V_a + V_b + V_c \qquad (A.4)$$

where

$$V_a = \pi r_e^2\left[\frac{\pi}{2}(r+r_e) - \frac{2}{3}r_e\right] \qquad (A.4a)$$

$$V_b = \pi r_e^2[-(r+r_e)\sin\alpha\cos\alpha + \tfrac{2}{3}r_e\sin\alpha\cos^2\alpha] \qquad (A.4b)$$

$$V_c = \pi r_e^2[(r+r_e)(-\alpha+\sin\alpha\cos\alpha) + \tfrac{2}{3}r_e\sin^3\alpha] \qquad (A.4c)$$

Substituting Eqs. (*A*.4*a*)–(*A*.4*c*) into Eq. (*A*.4),

$$V_{\rm II} = \pi\left[r_e^2(r+r_e)\left(\frac{\pi}{2}-\alpha\right) - \frac{2}{3}r_e^3(1-\sin\alpha)\right] \qquad (A.5)$$

$V_{\rm III}$ is the combination of cylinders, cones and rotated pies, as shown in Fig. 12.

$$V_{\rm III} = V_{\rm NBFH} + V_{\rm CDEF} - V_{\rm ABCM} - V_{\rm MCD} - V_{\rm KGED} - V_{\rm JKGH} \qquad (A.6)$$

where

$$V_{\rm NBFH} = \pi R^2 \Delta r/\tan\alpha \qquad (A.6a)$$

$$V_{\rm ABCM} = \pi[R^2 - (r-\Delta r+r_e)^2]\cdot r_e \qquad (A.6b)$$

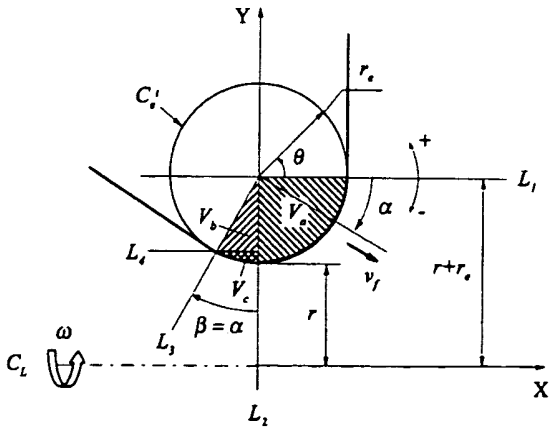

Fig. 11 Calculation of $V_{\rm II}$

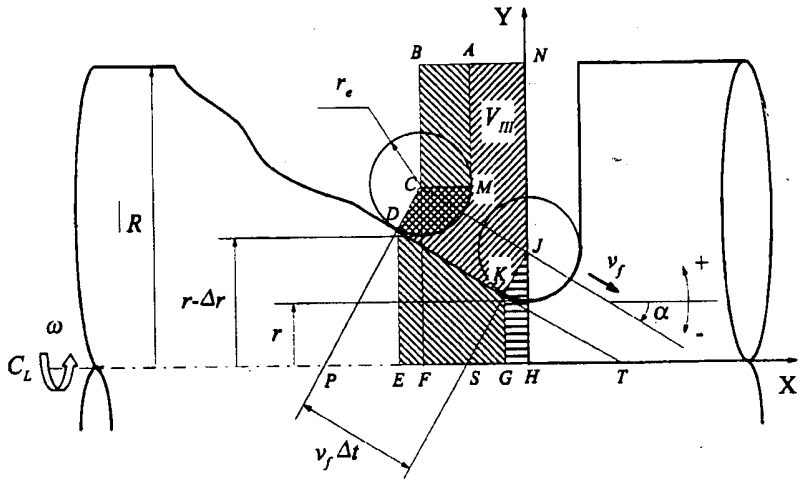

Fig. 12 Calculation of V_{III}

$$V_{CDEF}=V_{PFC}-V_{PED}=-\tfrac{1}{3}\pi[(r-\Delta r+r_e)^3-(r-\Delta r+r_e-r_e\cos\alpha)^3]\tan\alpha \quad (A.6c)$$

$$V_{KDEG}=V_{TDE}-V_{TKG}=-\tfrac{1}{3}\pi[(r-\Delta r+r_e-r_e\cos\alpha)^3-(r+r_e-r_e\cos\alpha)^3]/\tan\alpha \quad (A.6d)$$

$$V_{JKGH}=V_{SHJ}-V_{SGK}=-\tfrac{1}{3}\pi[(r+r_e)^3-(r+r_e-r_e\cos\alpha)^3]\tan\alpha \quad (A.6e)$$

$$V_{MCD}=\pi\left[r_e^2(r-\Delta r+r_e)\left(\frac{\pi}{2}-\alpha\right)-\frac{2}{3}r_e^3(1-\sin\alpha)\right] \quad (A.6f)$$

Substituting the formula of V_I, V_{II}, and V_{III} into Eq. (A.2), V can be expressed as:

$$V=-\pi\left(\frac{1}{3\tan\alpha}\right)\cdot(\Delta r)^3+\pi\left[r\frac{1}{\tan\alpha}+r_e\left(\frac{1}{\tan\alpha}-\frac{1}{\sin\alpha}+1\right)\right]\cdot(\Delta r)^2+\pi\left[(R^2-r^2)\frac{1}{\tan\alpha}+2rr_e\left(\frac{1}{\sin\alpha}-\frac{1}{\tan\alpha}-1\right)+r_e^2\left(\frac{2}{\sin\alpha}-\frac{2}{\tan\alpha}-2-\alpha+\frac{\pi}{2}\right)\right]\cdot\Delta r \quad (A.7)$$

Substituting Eq. (A.1) into Eq. (A.7),

$$\mathrm{MRR}=\lim_{\Delta t\to 0}\frac{V}{\Delta t}=v_f\cdot\pi\left[(R^2-r^2)\cos\alpha+2rr_e(1-\sin\alpha-\cos\alpha)+r_e^2\left(2-2\cos\alpha+\left(\frac{\pi}{2}-2-\alpha\right)\sin\alpha\right)\right] \quad (A.8)$$

References

[1] Masuzawa, T., Fujino, M., Kobayashi, K., and Suzuki, T., 1985, "Study on Micro-Hole Drilling by EDM," Bull. Jpn. Soc. Precis. Eng., **20**(2), pp. 117–120.

[2] Masuzawa, T., Fujino, M., Kobayashi, K., Suzuki, T., and Fujii, H., 1986, "Wire Electro-Discharge Grinding System for Machining Very Fine Rods," *International Conference on Computer-Aided Production Engineering, Edinburgh*, pp. 247–254.

[3] Kuo, C.-L., Masuzawa, T., and Fujino, M., 1992, "High-Precision Micronozzle Fabrication," *IEEE Micro Electro Mechanical Systems '92, Travemunde Germany*, Feb. 4–7, pp. 116–121.

[4] Masuzawa, T., Kuo, C.-L., and Fujino, M., 1994, "A Combined Electrical Machining Process for Micronozzle Fabrication," CIRP Ann., **43**, pp. 189–192.

[5] Langen, H. H., Masuzawa, T., and Fujino, M., 1995, "Modular Method for Microparts Machining and Assembly with Self-Alignment," CIRP Ann., **44**, pp. 173–176.

[6] Sun, Xi-Qing, Masuzawa, T., and Fujino, M., 1996a, "Micro Ultrasonic Machining and its Applications in MEMS," Sensors and Actuators, **A57**, pp. 159–164.

[7] Sun, Xi-Qing, Masuzawa, T., and Fujino, M., 1996b, "Micro Ultrasonic Machining and Self-Aligned Multilayer Machining/Assembly Technologies for 3D Micromachines," *Proceedings of the IEEE Micro Electro Mechanical Systems (MEMS) 1996*, Piscataway, NJ, pp. 312–317.

[8] Masuzawa, T., and Tonshoff, H. K., 1997, "Three-Dimensional Micromachining by Machine Tools," CIRP Ann., **46**, pp. 621–628.

[9] Yu, Z. Y., Masuzawa, T., and Fujino, M., 1998, "Micro-EDM for Three-Dimensional Cavities-Development of Uniform Wear Method," CIRP Ann., **47**, pp. 169–172.

[10] Rajurkar, K. P., and Yu, Z. Y., 2000, "3D Micro-EDM Using CAD/CAM," CIRP Ann., **49**, pp. 127–130.

[11] Slocum, A. H., 1992, *Precision Machine Design*, Prentice Hall.